

# LEMIX: Unified Scheduling for LLM Training and Inference on Multi-GPU Systems

Yufei Li   Zexin Li   Yinglun Zhu   Cong Liu  
University of California, Riverside  
{yli927, zli536, yzhu, congl}@ucr.edu

**Abstract**—Modern deployment of large language models (LLMs) frequently involves both inference serving and continuous retraining to stay aligned with evolving data and user feedback. Common practices separate these workloads onto distinct servers in isolated phases, causing substantial inefficiencies (e.g., GPU idleness) and delayed adaptation to new data in distributed settings. Our empirical analysis reveals that these inefficiencies stem from dynamic request arrivals during serving and workload heterogeneity in pipeline-parallel training. To address these challenges, we propose LEMIX, a system for *co-locating* and managing concurrent LLM serving and training workloads. LEMIX integrates offline profiling, execution prediction mechanisms, and runtime scheduling to dynamically adapt resource allocation based on workload characteristics and system conditions. By understanding task-specific behaviors and co-execution interference across shared nodes, LEMIX improves utilization and serving quality without compromising serving responsiveness. Our evaluation shows that LEMIX improves throughput by up to  $3.53\times$ , reduces inference loss by up to  $0.61\times$ , and delivers up to  $2.12\times$  higher response time SLO attainment over traditional separate setups. To our knowledge, this is the first work to uncover and exploit the opportunities of joint LLM inference and training, paving the way for more resource-efficient deployment of LLMs in production environments.

## I. INTRODUCTION

Recent advances in large language models (LLMs) have underscored the importance of *continuous* adaptation to maintain alignment with evolving data and user feedback [1–3]. Techniques like test-time training [4, 5] exemplify the potential for LLMs to improve dynamically during deployment. However, achieving this adaptability requires *concurrent* training and inference workloads, which are traditionally partitioned and separated across dedicated infrastructures [6–8]. For instance, platforms such as Amazon SageMaker provide isolated environments for training and serving, where models are periodically retrained on new data and redeployed to inference endpoints [9]. While this SEPARATE setup simplifies management, it inherently results in resource inefficiency.

**Potential resource inefficiencies.** In distributed systems, resource under-utilization arises from both independent training and inference workflows. On the inference side, advanced serving systems [10–16] employ continuous batching [17] to handle dynamic request arrivals. Although these approaches improve throughput and response times under high traffic, they often assume sustained demand, leading to *serving idleness* during off-peak periods when resources remain frequently inactive. On the training side, parallelism techniques [18–24] are widely used to accommodate the resource demands

of LLMs by vertically partitioning computations across distributed systems. While these approaches improve utilization, they introduce sequential dependencies in forward and backward passes, causing *pipeline idleness* (a.k.a. “bubbles”) [25] during execution.

Figure 1a empirically demonstrates inefficiencies of the SEPARATE strategy running a Llama-8B model [26] across four nodes (servers) with eight A100 GPUs. Each model instance is divided into two stages on a node, with two nodes allocated to serving inference requests based on real-world traces from the LMSYS Chatbot Arena [27, 28], and the remaining two nodes dedicated to training. We observe that inference suffers from low average GPU utilization at just 13.62% due to inactive request periods. Despite a higher utilization of 29.16%, distributed training exhibits interleaving patterns caused by pipeline idle intervals.

**Joint inference and training.** To address these inefficiencies, we first propose NAIVEMIX, a strategy that *co-locates* training and inference workloads on shared nodes via a simple round-robin (RR) policy. As shown in Figure 1d, NAIVEMIX increases the average GPU utilization by around 8% over SEPARATE through dynamically interweaving inference and training tasks. This increased utilization arises from the overlap of inference and training workloads, enabling otherwise idle GPU resources to be utilized more efficiently. Moreover, NAIVEMIX enables *on-the-fly* adaptation for concurrent workloads, where training updates immediately enhance the accuracy of subsequent co-located inference tasks, eliminating the delay associated with periodic inter-node model synchronization [16] required in SEPARATE setups.

However, naïve co-location alone offers limited gains, with NAIVEMIX achieving an average of 31.88% GPU utilization. One reason is that NAIVEMIX is not sufficiently *fine-grained*, leading to co-execution interference between asynchronous workloads. For example, unfinished training backward passes can race and delay subsequent inference requests, especially under high traffic. Furthermore, real-world workloads exhibit *dynamic* request arrival patterns [12], with *heterogeneous* request lengths [13, 14] that exacerbate execution delays and additional GPU idle periods. During high traffic, these inefficiencies compound as memory contention induces prolonged overruns, causing degraded responsiveness and potential service level objective (SLO) violations [29].

**A comprehensive solution.** Recognizing these challenges, we propose LEMIX, a fine-grained framework for co-operating

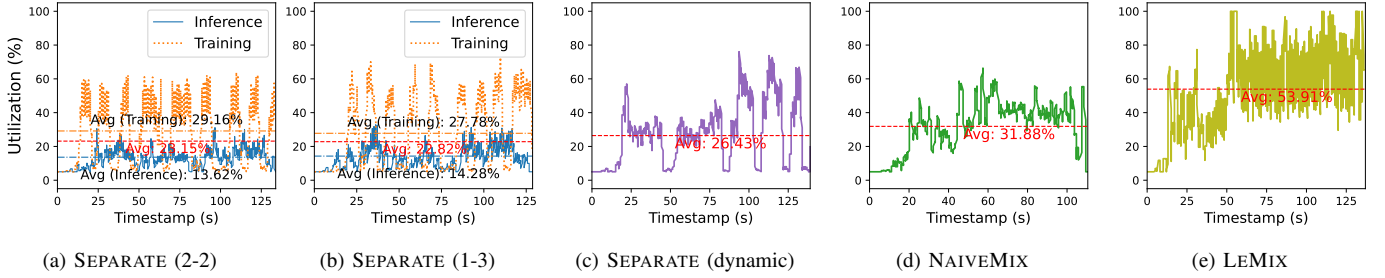


Fig. 1: GPU utilization of three SEPARATE setups, NAIVEMIX, and LEMIX when deploying Llama-8B on eight A100 GPUs under LMSYS workloads. SEPARATE (2-2) and SEPARATE (1-3) dedicate 2 (1) nodes to inference and 2 (3) nodes to training, while SEPARATE (dynamic) alternates between these configurations based on request rates. NAIVEMIX and LEMIX co-locate both workloads across all four nodes.

LLM training and inference workloads in distributed systems. LEMIX aims to: (1) maximize resource utilization, (2) improve inference accuracy via continuous retraining, and (3) meet response time SLO. Unlike NAIVEMIX, LEMIX integrates task-specific execution awareness and runtime adaptability to dynamically balance these objectives.

Specifically, LEMIX leverages an offline profiler to gather latency and memory coefficients on each hardware (§IV-A). These profiled results enable the system to speculate the execution behaviors of online tasks and their system-wide impact (§IV-B), while also providing actionable insights for co-optimizing multiple objectives during resource allocation (§IV-C) and runtime execution scheduling (§IV-D). As a result, LEMIX can *consolidate* workloads onto fewer nodes during periods of light demand—such as low request rates or reduced training intensity—without compromising SLO compliance. As shown in Figure 1e, LEMIX significantly improves the average GPU utilization by around 22% over NAIVEMIX, through fine-grained node partitioning and runtime scheduling based on real-time workload conditions (e.g., request rate, retraining burden). This adaptability ensures LEMIX remains robust in real-world scenarios with dynamic arrival patterns and heterogeneous computational demands.

**Contributions.** We evaluate LEMIX on diverse models and hardware, including three GPT models on A6000 GPUs and three Llama models on A100 GPUs, leveraging model parallelism under both synthetic and real workload traces. LEMIX delivers up to  $3.53\times$  higher throughput,  $0.61\times$  lower inference loss, and  $2.12\times$  higher SLO attainment over SEPARATE under various conditions. Our contributions are:

- To our knowledge, this is the first study of concurrent LLM training and inference in distributed systems, unveiling inefficiencies in both SEPARATE (§II) and NAIVEMIX (§III) setups and identifying optimization opportunities.
- We propose LEMIX, a dynamic task-specific framework that coordinates mixed workloads, optimizing resource utilization, inference accuracy, and response SLO compliance under diverse real-time conditions (§IV).
- We extend the scope of co-location techniques to support a wide range of LLM serving (e.g., autoregressive generation) and parallel training (e.g., data parallelism) scenarios, demonstrating the generality of LEMIX (§V).

## II. BACKGROUND AND ANALYSIS OF SEPARATE

Recent surge in deploying LLMs for continuous user interaction [30] has necessitated effective strategies for handling concurrent training and inference tasks. These workloads span responding to user queries and retraining aimed at aligning LLM outputs with human preferences [31, 32] and ensuring factuality [33, 34]. A widely adopted approach to manage such workloads in distributed systems is the SEPARATE strategy, which dedicates servers in different phases to either inference or training tasks [7]. While this setup simplifies management and ensures inference accuracy, it exhibits resource inefficiencies under realistic workload conditions.

### A. System Model and Terminology

Stage	Sharded sub-model (e.g., layers 0-8) on a specific GPU.
Node	A single server containing multiple GPUs (e.g., $8\times A100$ ).
Task	An inference or training operation across stages within a node, where an inference task is forward-only, while a training task includes a forward + backward.
Batch	Internal mini-/micro-batching strategies within each task. They do not affect how LEMIX views or schedules tasks across nodes.

TABLE I: List of key terms used in the paper.

Table I includes a system model, defining key terms such as task, node, and stage of execution in this paper. We assume tasks are independent (no inter-task communication), and their arrivals are externally triggered (e.g., by user queries).

### B. Empirical Analysis of SEPARATE

Figure 1b highlights the limitation of SEPARATE under another static “1-3” partition, allocating one node for inference and three nodes for training. While this setup slightly increases the average inference utilization to 14.28%, training utilization drops to 27.78% compared to the “2-2” partition, leading to negligible overall gains. These observations suggest that altering the fixed partition of nodes alone provides limited benefits.

To address workload variability, we further evaluate a more adaptive *dynamic* SEPARATE strategy that alternates between “1-3” and “2-2” setups based on request rates (“1-3” for less than 50 rps and “2-2” otherwise), as shown in Figure 1c. However, even with these adjustments, the average utilization only improves marginally to 26.43%, indicating the persistent

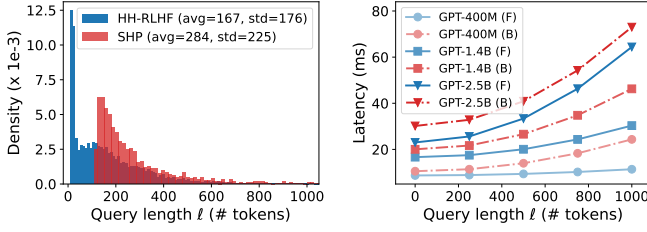


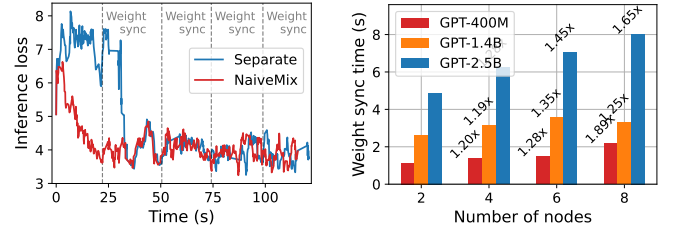
Fig. 2: *Left*: The length distribution (w/ standard deviation) of two datasets and *Right*: the forward (F) and backward (B) latency running GPT models on a single RTX A6000 GPU.

inefficiencies of partitioning regardless of node allocation. These inefficiencies stem from two key challenges: serving idleness due to dynamic request arrivals and training pipeline idleness caused by workload heterogeneity.

### C. Two Main Sources of Inefficiencies in SEPARATE

**Serving idleness in dynamic environments.** Modern LLM deployments operate in a *multitenant* environment with highly *dynamic* request patterns across multiple node instances [12]. To address the significant memory demands of LLM inference, model parallelism (MP) [35] and continuous batching [17] are widely employed, wherein each GPU hosts a sharded model slice (*a.k.a.* stage) and sequentially executes forward passes of a mini-batch to reduce latency through statistical multiplexing [23]. While MP enables serving large models on memory-constrained devices, it exacerbates GPU idle periods during light traffic. For example, under low request rates in Figure 4a, idle GPU intervals, such as between tasks 2 and 3 on Node 1, are frequent, leaving significant portions of the pipeline underutilized. This inefficiency becomes more pronounced in large-scale distributed systems, where per-node request rate is even lower during off-peak hours [36].

**Pipeline idleness from workload heterogeneity.** To meet the high computational costs of LLM training, pipeline parallelism (PP) [21, 25] extends MP to divide mini-batches into smaller micro-batches that are processed in parallel to maximize utilization. While asynchronous PP (A-PP) [18] theoretically minimizes idleness by continuously processing micro-batches without flushing, LLM tasks with context-specific inputs introduce a unique challenge: *workload heterogeneity*. As shown in Figure 2, real-world user preference alignment datasets: HH-RLHF [37] and SHP [38], exhibit significant variability in query lengths, leading to diverse forward and backward latencies due to attention computation [39]. This variability disrupts the seamless execution of A-PP, as overlapping forward and backward passes contend for GPU resources, leading to execution delays and increased idle periods. For example, on Node 2 of Figure 4a, task 2' ( $\nabla$ ) begins execution on GPU2 (S2) much later due to interference from the backward pass of task 1'. Similarly, task 5' ( $\diamond$ ) cannot leverage the pipeline idle periods left by task 3' or task 4'. This postponed inter-stage execution is termed as *far dependency* [22], as opposed to *immediate dependency* when tasks have the same lengths and execute without delays. These



(a) Continuous vs. periodic retrain (b) Inter-node sync latency

Fig. 3: Real data showcasing (a) inference loss over time and (b) weight synchronization latency across nodes for SEPARATE.

inefficiencies accumulate over time, resulting in prolonged E2E latency and fragmented memory. Although increasing concurrency, such as splitting mini-batches into more micro-batches, partially mitigates idleness, the associated communication overhead [21] and far dependencies impose fundamental limits on system efficiency.

## III. MOTIVATION OF WORKLOAD CO-LOCATION

The evolving in-context learning capabilities of LLMs [1] present an opportunity to optimize resource utilization by learning while serving inference requests. We propose that *co-locating* training and inference workloads on shared resources mitigate the inefficiencies inherent in SEPARATE. A baseline strategy, NAIVEMIX, assigns tasks to nodes using a fair Round-Robin (RR) policy based on their in-queue order, as shown in Figure 4b. Inference tasks are queued according to their online arrival times, while training tasks are queued according to the first-stage (S1) forward end times of previous training tasks. For example, in the right part of Figure 4, the first four tasks enqueued are 1', 1, 2, 2'. Consequently, NAIVEMIX co-locates tasks 1' and 2 on Node 1, while allocating tasks 1 and 2' to Node 2 for execution.

### A. Advantages of NAIVEMIX

**De-fragmentation.** NAIVEMIX effectively enhances resource utilization compared to SEPARATE by reducing idle periods across various real-time conditions:

- At low request rates, NAIVEMIX alleviates serving idleness by running training workloads within the arrival gaps. For example, majority of training tasks 3' and 4' on Node 2 are executed in the interval between inference tasks 1 and 3.
- At high request rates, NAIVEMIX reduces pipeline idleness by inserting inference workloads into underutilized stages of training pipelines. For example, task 8 on Node 1 utilizes the idle pipeline period left by tasks 4' and 5'.

**Latency reduction.** By distributing training tasks across potentially more nodes, NAIVEMIX naturally relaxes the far dependencies caused by forward-backward interference in A-PP. For example, task 5' completes much earlier than in SEPARATE training. These optimizations in utilization consequently reduces E2E latency—the cumulative execution time across all nodes for executing a given workload, enabling more GPU time to be devoted to actual computations.

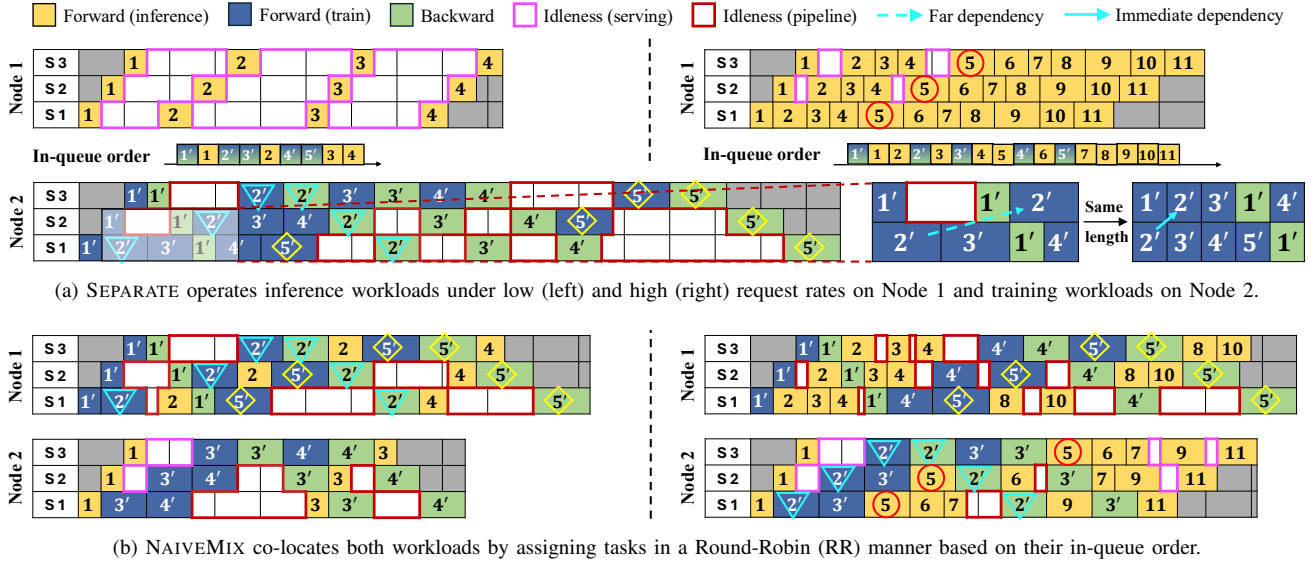


Fig. 4: Comparison of (a) SEPARATE and (b) NAIVEMIX under *Left*: low request rates and *Right*: high request rates on a two-node cluster. For simplicity, we present one micro-batch for each mini-batch.

**Enhanced serving quality.** NAIVEMIX continuously improves inference accuracy by co-locating both workloads, which allows model instances to be updated in near real-time, benefiting serving quality on shared nodes. For example, under low traffic, the performance of task 4 on Node 1 is enhanced due to updates after the backward pass of training task 1'. Conversely, as shown in Figure 3a, SEPARATE requires periodically synchronizing (e.g., checkpointing) updated weights [16] from training to inference nodes, sacrificing serving quality before each communication. The synchronization overhead is also non-trivial and grows with model size and cluster scale (e.g., the number of nodes), as illustrated in Figure 3b.

### B. Optimization Opportunities

While NAIVEMIX alleviates multi-source inefficiencies of SEPARATE, its effectiveness is limited due to coarse-grained task-agnostic execution awareness.

**Suboptimal resource utilization.** NAIVEMIX still leaves spaces for utilization optimization. For example, low *training rate*—the proportion of training tasks in the queue—limits the reduction in serving idleness when insufficient training tasks are available to reduce the serving idleness if distributed across more nodes, such as between tasks 2 and 4 on Node 1 in Figure 4b under low request rates. Moreover, workload heterogeneity remains a challenge. In Figure 4b, task 1 is assigned to Node 2 under low request rates. However, allocating task 1 to Node 1 would instead utilize the idle periods left by task 1'. Figure 5a validates this impact on NAIVEMIX's utilization across subsets with different length variances sampled from HH-RLHF [37]. We observe a consistently decreasing GPU utilization under highly-variable query lengths, particularly under heavy traffic. These inefficiencies highlight the need for a *fine-grained* policy that accounts for task-specific contributions to GPU idle periods during resource allocation.

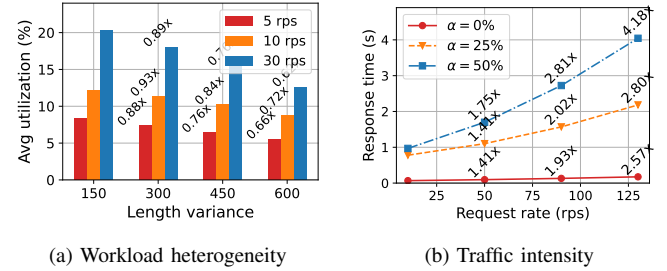


Fig. 5: Impact of (a) workload heterogeneity on utilization under different request rates and (b) request rate on serving responsiveness under different training rates  $\alpha$ .

**Prolonged serving response time.** Naïve co-location inevitably enlarges inference response times due to resource contention between training and serving, especially during high-traffic periods. In Figure 4b, task 5 (○) on Node 2 takes longer to complete compared to its execution on Node 1 under SEPARATE. Our empirical results of deploying GPT-2.5B under NAIVEMIX in Figure 5b show a prolonged inference response time as request and training rates grow, due to more frequent co-execution interference. A fine-grained approach is needed to estimate task-specific response times and *prioritize* inference tasks that risk violating SLO targets.

**Memory contention in overloaded systems.** NAIVEMIX lacks runtime awareness of resource availability, leading to potential memory contention [40] when concurrent workloads interfere in their pipelines. Under heavy traffic, autoregressive inference workloads may overlap with computation-intensive backward passes, especially when longer sequences and KV cache [41] are involved. These simultaneous workloads can trigger memory overruns and further extend latencies, which is compounded by the unpredictable behaviors of accelerators under high load, such as non-deterministic scheduling delays and memory fragmentation [42]. Therefore, a runtime profiler





---

**Algorithm 1** COMPUTEIDLENESS

---

```

1: Input: number of GPUs per node  $S$ , trace queues  $Q^n := Q_{\text{train}}^n \cup Q_{\text{inference}}^n$  for each node  $n$ , new task batch:  $\{a, \ell, C\}$ 
2: Parameters: forward and backward coefficient  $\eta_F^n, \eta_B^n$ 
3: Initialize:  $\Pi \leftarrow 0$ ,  $\text{task}_{\text{prev}} \leftarrow Q^n[-1]$ ,  $Q_{\text{temp}} \leftarrow Q_{\text{train}}^n$ 
4: for each stage  $s \in \{1 \dots S\}$  do
5:    $\text{task.start}_f^s \leftarrow \max(\text{task.end}_f^{s-1}, \text{task}_{\text{prev}}.\text{end}_f^s)$ 
6:    $\text{task.end}_f^s \leftarrow \text{task.start}_f^s + \eta_F^n \cdot C \cdot \ell^2$ 
7:    $\text{offset} \leftarrow 0$ 
8:   while  $Q_{\text{temp}} \neq \emptyset$  do
9:      $\text{task}_{\text{train}} : \{a_{\text{train}}, \ell_{\text{train}}, C_{\text{train}}\} \leftarrow Q_{\text{temp}}.\text{dequeue}()$ 
10:    if  $\text{task.end}_f^s \leq \text{task}_{\text{train}}.\text{start}_b^s$  then
11:       $Q_{\text{temp}} \leftarrow Q_{\text{temp}} \cup \{\text{task}_{\text{train}}\}$ 
12:      break
13:     $\text{task.start}_f^s \leftarrow \max(\text{task.start}_f^s, \text{task}_{\text{train}}.\text{end}_b^s)$ 
14:     $\text{task.end}_f^s \leftarrow \text{task.start}_f^s + \eta_F^n \cdot C \cdot \ell^2$ 
15:    if  $\text{task}_{\text{prev}}.\text{end}_f^s \leq \text{task}_{\text{train}}.\text{start}_b^s$  then
16:       $\text{offset} \leftarrow \text{offset} + \eta_B^n \cdot C_{\text{train}} \cdot \ell_{\text{train}}^2$ 
17:    if  $s = 1 \wedge \text{CHECKEXECUTED}(\text{task}_{\text{train}}, s)$  then
18:      Remove  $\text{task}_{\text{train}}$  from  $Q_{\text{train}}^n$ 
19:     $\Pi \leftarrow \Pi + \text{task.start}_f^s - \text{task}_{\text{prev}}.\text{end}_f^s - \text{offset}$ 
20:  $R \leftarrow \text{task.end}_f^S - a$ 
21: return  $\Pi, R$ 

```

---

Their calculation is detailed in Algorithm 1.

**Initialization.** For each node  $n$ , LEMIX maintains two trace queues  $Q_{\text{train}}^n$  and  $Q_{\text{inference}}^n$ , which track the execution paths of ongoing tasks. The forward path of a new task is initialized based on the end time of the preceding task  $\text{task}_{\text{prev}}$  and the immediate dependency. For each stage  $s$ , its forward start time is the later of two events: its forward end time in the preceding stage  $s - 1$  or  $\text{task}_{\text{prev}}$ 's forward end time in the current stage (line 5). The forward end time is incremented by an estimated forward execution latency (line 6).

**Far dependency rescheduling.** To efficiently account for far dependencies caused by co-execution interference, LEMIX introduces a temporary queue,  $Q_{\text{temp}}$ , which tracks pending training tasks in  $Q_{\text{train}}^n$ . For each training task in  $Q_{\text{temp}}$ :

- If the current forward can finish before the backward of the training task begins, the stage executes the forward pass during this idle pipeline period. The task is then reinstated in  $Q_{\text{temp}}$  for subsequent stages (lines 10-12).
- Otherwise, the forward start time is postponed to the backward end time of this interfered task, and the forward end time is recalculated accordingly (lines 13-14). Particularly, if this training task completes its backward pass, it is removed from the node queue  $Q_{\text{train}}^n$  to avoid recomputation in subsequent stages (lines 17-18).

All backwards executed between the previous and current forward (e.g., task 1' on Node 1 in Figure 7) are recorded, and their cumulative execution times are subtracted from the serving intervals to yield  $\Pi$  (line 15-19). The response time  $R$  is estimated after forward path planning (line 20).

**Backward planning.** For tasks requiring training, the backward paths are initialized immediately after the forward paths. The backward start and end times are sequentially computed for each stage in reverse order, propagating back through the

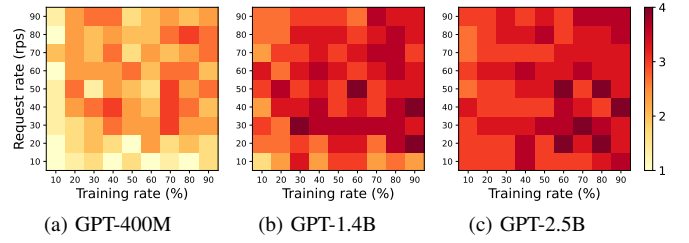


Fig. 8: Number of allocated nodes (out of 4) for LEMIX when processing concurrent workloads under various setups.

pipeline and maintaining a dependency chain between stages until the traversal ends. The planned backward paths aid in forecasting subsequent tasks before the execution.

### C. Hierarchical Resource (Node) Allocation

Based on anticipated idle periods and response times for each node, LEMIX optimizes resource allocation to address three objectives—maximizing resource utilization, minimizing serving response time, and improving serving quality under dynamic workload conditions. To achieve this, LEMIX employs a two-level hierarchical policy:

- **Task-level (local):** New tasks are assigned to nodes with the highest priority scores, calculated using heuristic balancing the three objectives. For example, the new task in Figure 7, if assigned to Node 2, would produce lower  $\Pi$  and  $R$ .
- **Queue-level (global):** LEMIX dynamically adjusts task priorities in the global task queue, deprioritizing training tasks that risk delaying subsequent inference tasks (and violating SLO goals) at high request rates.

**Task-level multi-objective node allocation.** LEMIX defines *idleness profit* (IP) to capture the utilization benefit of accommodating the incoming task to a specific node

$$\text{IP} = -\max \left\{ \frac{\Pi}{S} - (a - a_{[-1]}), \tau \right\}, \quad (1)$$

where  $a - a_{[-1]}$  represents the *inter-arrival interval* between the preceding and incoming task,  $S$  is the number of GPUs per node, and  $\tau$  is a threshold. IP penalizes nodes with large increased idle periods relative to arrival intervals, enabling LEMIX to adapt to dynamic request rates—a key characteristic of modern LLM-serving systems [12].

LEMIX incorporates *length consistency* (LC), which quantifies how well a task with query length  $\ell$  aligns with a node's historical workload, as the serving quality heuristic

$$\text{LC} = \frac{1}{\sigma_{<a}\sqrt{2\pi}} \exp \left\{ -\frac{(\ell - \mu_{<a})^2}{2\sigma_{<a}^2} \right\}, \quad (2)$$

where  $\mu_{<a}$  and  $\sigma_{<a}$  are the mean and standard deviation for previously executed tasks on the node. Higher LC scores align tasks with a node's workload profile, which has been shown benefiting training convergence [43, 44] and minimizing GPU idle periods caused by workload heterogeneity (§III-B). For inference tasks assigned to different nodes, LEMIX minimizes cache miss rate by prioritizing *prefix reuse* [45] for length-bucketed queries, which keeps most requests on warm caches.

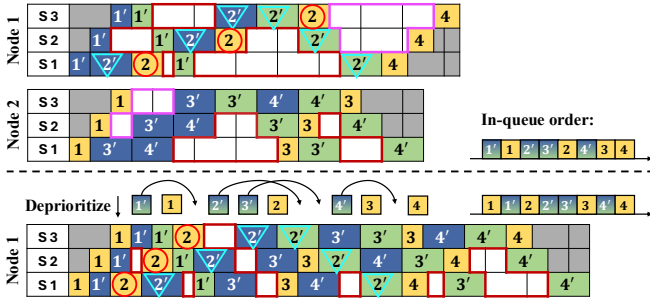


Fig. 9: An illustration of how *Bottom*: LEMIX consolidates workloads from *Top*: NAIVEMIX into one node to optimize utilization while maintaining SLOs via deprioritization.

The node priority score integrates the three objectives

$$f = \frac{IP + \lambda_2 \cdot LC}{\lambda_1 \cdot R}, \quad (3)$$

where  $\lambda_1$  and  $\lambda_2$  balance the trade-off between response latency  $R$  and serving quality heuristic. Tasks are assigned to nodes with the highest priority scores, dynamically updating the node queues. This priority-based mechanism enables *workload consolidation*, dynamically adjusting the number of active nodes based on real-time conditions, as shown in Figure 8. Key observations include:

- Higher training rates lead to an increased  $II$ , as more unfinished backward passes create contention for resources, reducing  $IP$  and  $f$  for allocated nodes. This shift tasks to new nodes to alleviate resource contention.
- As request rates rise, arrival intervals shorten, amplifying  $II$  due to the added interference caused by workload heterogeneity, again lowering  $f$  and favoring new nodes.
- Larger model sizes exacerbate workload heterogeneity, as they magnify  $\eta_F^n$  and  $\eta_B^n$  (Figure 2). This increase in  $II$  reduces the profitability ( $IP$ ) of assigning tasks to allocated nodes, instead favoring new nodes.

**Queue-level task prioritization.** While local-level selection optimizes individual assignment, it neglects the inter-task impact that arises under high-traffic scenarios. In such cases, both bursty inference requests and training tasks compete for shared resources, preempting subsequent inference tasks and risking SLO violations. To maintain serving throughput, LEMIX *deprioritizes* training tasks if the minimum estimated response time of its subsequent enqueued inference task  $task_{next}$  across all nodes violates the SLO target

$$\min_{1 \leq n \leq N} \left\{ \max_{task \in Q^n} \{task_{next}.end_f^s\} + \eta_F^n \cdot C' \cdot \ell'^2 \right\} - a' > \tau_R, \quad (4)$$

where  $C'$ ,  $\ell'$ ,  $a'$  are the batch size, query length, and arrival time of  $task_{next}$ .  $\tau_R$  is a response SLO goal, e.g.,  $5 \times$  inference latency. In Figure 9, LEMIX defers training tasks  $2'$  and  $3'$  on Node 1, as either would significantly delay inference task 2. These severe delays, if arise from far dependencies in preceding tasks (e.g., task  $2'$ ), also indicate under-utilization and could be optimized through this deprioritization process. Practitioners can set different SLO goals to balance serving responsiveness and training efficiency. A larger  $\tau_R$  increases

## Algorithm 2 EXECUTETASKMEMORYAWARE

```

1: Input: number of GPUs per node  $S$ , task queues  $Q^n := Q_{train}^n \cup Q_{inference}^n$  for each node  $n$ .
2: Parameters: Memory utilization threshold  $M_{threshold}$ , check interval  $\Delta_t$ , and maximum wait time  $T_{max}$ 
3: while  $Q^n \neq \emptyset$  do
4:    $task \leftarrow Q^n.dequeue()$ 
5:   for each stage  $s \in \{1 \dots S\}$  do
6:      $wait \leftarrow 0$ 
7:     while not MEMORYAVAILABLE( $n, s, M_{threshold}$ ) do
8:        $wait \leftarrow wait + \Delta_t$ 
9:       if  $wait \geq T_{max}$  then
10:        Offload KV cache of  $task$  from GPU  $s$ 
11:        break
12:     if MEMORYAVAILABLE( $n, s, M_{threshold}$ ) then
13:       FORWARD( $task, s$ )
14:       Calibrate  $\langle task.start_f^s, task.end_f^s \rangle \in Q^n$ 
15:       if  $s = S \wedge task.require\_backward$  then
16:         BACKWARD( $task$ )
17:         Calibrate  $\langle task.start_b^s, task.end_b^s \rangle \in Q_{train}^n$ 

```

delay tolerance, preserving training priority for improving serving quality, while a smaller  $\tau_R$  penalizes SLO violations more strictly, prioritizing serving responsiveness.

### D. Runtime Memory-Aware Scheduling

After dispatching tasks to specific nodes, LEMIX coordinates all ongoing tasks with the new one on each node, ensuring reliable service under dynamic traffic. To handle the risk of memory overruns—especially critical when co-locating computation-intensive batched operations—LEMIX incorporates a runtime scheduler that maintains SLOs without sacrificing resource efficiency. Memory overruns occur when overlapping pipelines exceed the system’s available memory, potentially delaying inference generation or disrupting training operations. To preemptively manage memory and mitigate these issues, LEMIX employs a stage-level *wait-or-drop* policy, as shown in Algorithm 2.

**Wait-or-drop with execution calibration.** Runtime monitoring is conducted before each forward on a stage. When an incoming task’s memory demands exceeds the device’s capacity due to concurrency, it is placed in a temporary wait state (lines 6-8). By deferring execution until enough memory is available, this phase prevents immediate conflicts without disrupting ongoing tasks. It is particularly beneficial for autoregressive generation tasks, where low latency is critical. If the memory remains constrained beyond a profiled threshold  $T_{max}$ , LEMIX *offloads* intermediate activations and KV cache [41] to CPU [46] to scale down memory demands and free resources for inference to attain SLOs (lines 9-10). After execution, forecasted paths (§IV-B) in the node queues are *calibrated* by the execution traces (lines 13–17), facilitating future task planning and scheduling optimization.

## V. IMPLEMENTATION AND DISCUSSION

### A. Implementation

LEMIX is built on top of vLLM [11] and DeepSpeed [47] for MP and PP, and FlashAttention [48] for memory optimiza-

tion during inference generation. We realize asynchronous execution of stages using Python *concurrent* library. Specifically, LEMIX employs a global scheduler that makes scheduling decisions oriented to the node instances, according to the priority and memory load of them. It invokes each node as a *multi-threaded* execution environment, where each thread is assigned to manage a stage of the instance pipeline. For each node, tasks are scheduled across these threads following the forward and backward dependencies. Each thread is responsible for coordinating and executing the forward and backward (if applicable) jobs for its assigned stage. Once the memory availability for a task is confirmed, the appropriate thread invokes the execution process.

### B. Model Update Synchronization

In SEPARATE, model on the final training node is periodically checkpointed (e.g., every 100 training tasks) and loaded onto inference nodes to ensure consistent serving quality.

Co-location methods, such as NAIVEMIX and LEMIX, adopt a *decentralized* strategy similar to federated learning where each node independently updates its local model instance based on its local training tasks. This setup resolves privacy concerns where sharing weight can be highly risky.

### C. Scalability and Distributed Architecture

We assume an implicit client-server architecture. Real-world LLM systems (like Azure, AWS) do not rely on a centralized scheduler for every request. Instead, they adopt a distributed, hierarchical architecture that scales efficiently to millions of requests per minute. LeMix operates on both *cluster-level* and *GPU-level*, with its global queue stored in a cluster, and each local queue stored in a server (node):

- **Front-end load balancers:** Distribute client requests geographically across server clusters (e.g., by regions, time zones) using stateless heuristics like round-robin or SLO-aware routing to handle high traffic volumes (e.g., 10k+ rps) without per-request scheduling.
- **Cluster-level scheduler:** LEMIX precisely allocate requests to specific servers within each cluster to coordinate training and inference tasks, which typically handles  $< 150$  rps. This aligns with our experimental setups and reflects the practical scale of resource allocation at the cluster level. As shown in analysis (§VI-F), LEMIX incurs negligible overhead under this workload.
- **GPU-level runtime scheduler:** Once tasks are assigned to a server, LEMIX manages execution using fine-grained techniques such as memory-aware batching, KV cache offloading, to optimize throughput and avoid OOM.

The efficiency of LEMIX is rooted in its lightweight design, enabling scalability in large-scale distributed systems. Task-specific execution planning involves forecasting idle periods and response times for incoming tasks. This step incurs an  $O(S)$  complexity per node, where  $S$  is the number of stages (GPUs) in the node. Resource allocation computes priority scores for all  $N$  nodes and selects the optimal node for each task, resulting in an  $O(N \cdot S)$  complexity. Memory-aware

---

### Algorithm 3 CONTINUOUSBATCHING

---

```

1: Input: Maximum batch size  $C$ , maximum waiting time  $T_w$ , task
   queue  $Q^n$  for a specific node  $n$ .
2: Initialize: batch  $B^n \leftarrow \emptyset$ , batch start  $T_{start} \leftarrow$  current time
3: while True do
4:   if  $B^n = \emptyset$  then
5:      $T_{start} \leftarrow$  current time
6:     while  $Q^n \neq \emptyset$  and  $|B^n| < C$  do
7:        $r \leftarrow \text{get\_next\_request}(Q^n)$ 
8:       if not  $r.\text{require\_backward} \wedge T_{start} + T_w > \text{current time}$ 
then
9:         Add  $r$  to  $B^n$  with padding (if necessary)
10:      else
11:        break
12:   if  $B^n \neq \emptyset$  then
13:     Execute batch  $B^n$  on node  $n$ 
14:      $B^n \leftarrow \text{filter\_finished\_requests}(B^n)$ 

```

---

scheduling adjusts task execution based on runtime conditions such as memory availability and task inter-dependencies, maintaining an  $O(S)$  overhead per node by only considering active queues. Overall, LEMIX’s end-to-end scheduling operates with  $O(N \cdot S)$  complexity across  $N$  nodes and  $S$  stages, ensuring efficient coordination even in large clusters.

### D. Autoregressive Generation

Serving requests are handled using continuous batching into mini-batches up to a maximum size  $C$  on a FCFS basis, as shown in Algorithm 3. To prevent excessive delays during low-traffic periods, a maximum waiting time  $T_w$  (defaulting to  $0.5 \times$  inference latency) ensures timely execution even when the batch size  $C$  is not reached. In particular, for autoregressive generation, we adopt hybrid iteration-level batching [17]. Each incoming request represents a prefilling workload, which is integrated with ongoing decoding workloads into mini-batches to improve throughput and responsiveness. In LEMIX, prefilling requests, which initialize new sequences, are allocatable across nodes based on our task assignment strategy, informed by execution predictions of continuously batched task on each node. Decoding requests, which extend prefilled contexts, operate continuously on the same node as their corresponding prefilling tasks, maintaining data locality and supporting dynamic scheduling, such as offloading, when memory bottlenecks arise.

## VI. EVALUATION

We evaluate LEMIX across different LLM sizes and workload conditions, including diverse request rates and training rates. Experimental results show that LEMIX consistently outperforms baseline systems in all scenarios, achieving up to  $3.53 \times$  higher throughput,  $0.61 \times$  lower inference loss, and  $2.12 \times$  higher SLO attainment compared to SEPARATE (§VI-B). We further delve into node-level latency and response time breakdown under real workloads, showcasing how LEMIX’s dynamic resource allocation enhances utilization and operational efficiency (§VI-C). The benefits of LEMIX become even more pronounced under high workload heterogeneity,



Name	Size	# Layers	Hidden size	Forward	Backward
GPT-400M	1.0GB	12	768	0.03s	0.04s
GPT-1.4B	2.3GB	24	1024	0.08s	0.09s
GPT-2.5B	4.5GB	36	1280	0.12s	0.14s
Llama-8B	13GB	32	4096	0.11s	0.15s
Llama-13B	26GB	40	5120	0.24s	0.36s
Llama-70B	132GB	80	8192	0.73s	1.05s

TABLE II: Model configuration and latency requirements.

where task-specific scheduling proves critical to performance gains (§VI-D). We also analyze fine-grained inference latency in different phases (§VI-E). Finally, we conduct ablation studies to provide deeper insights into its techniques (§VI-F).

### A. Experimental Setup

**Datasets and models.** We use two popular preference datasets targeting different alignment domains: HH-RLHF [37] (harmlessness) and SHP [38] (helpfulness), to mimic the serving and alignment fine-tuning of LLM deployment. Specifically, we sample 1,000 query-reference pairs in each online test to evaluate the model and system performance. In this work, we consider GPT [49] and Llama [26] family models of various sizes. Table II shows their detailed configurations.

**Testbed setups.** We use two testbed configurations. For GPT models, we use 4 servers, each equipped with 2 NVIDIA RTX 6000 Ada GPUs (48 GB), 64 AMD EPYC-7543 CPU cores, and 2 TB memory. For larger Llama models, we use 4 AWS EC2 servers, each equipped with 2 NVIDIA A100 Tensor Core GPUs (80 GB), connected with pairwise NVLINK.

**Synthetic workloads.** We mimic human requests as a Poisson process [23, 29, 43] and synthesize traces by sampling inter-arrival times from an exponential distribution with mean of the reciprocal of the various request rates. Tasks are sampled from the same dataset as training (e.g., SHP) to simulate online serving and retraining scenarios.

**Real workloads.** We further explore the effectiveness of LEMIX in more complex inference workloads constructed from the trace of LMSYS Chatbot Arena [27]—a real-world LLM serving platform for clients.

**Metrics.** We measure throughput as the average number of completed tasks per second and analyze the E2E latency across all nodes running the same amount of workloads, for utilization analysis. For serving quality, we evaluate the average inference decoding loss. For serving efficiency, we evaluate prefilling latency, i.e., time-to-first-token (TTFT), decoding latency, i.e., time-between-tokens (TBT) [13], and SLO attainment—proportion of inference tasks whose TTFT meet a SLO deadline of  $5\times$  forward latency [23].

**Baselines.** We compare LEMIX with three baselines as below:

- **SEPARATE** [22, 23]: Nodes are partitioned into training and inference nodes based on training rates  $\alpha$ .  $N_{\text{train}} = \lfloor N \cdot \alpha + 0.5 \rfloor$  nodes are dedicated to training and the remaining to inference to balance workloads. Each task is assigned to a training or inference node in a RR fashion.
- **MIX-RR** (NAIVEMIX): Tasks are assigned to nodes in a sequential RR order. This method ensures a uniform distribution of tasks across all nodes.

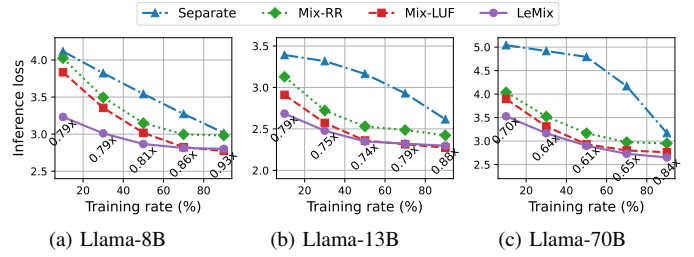


Fig. 10: Average inference loss at various training rates.

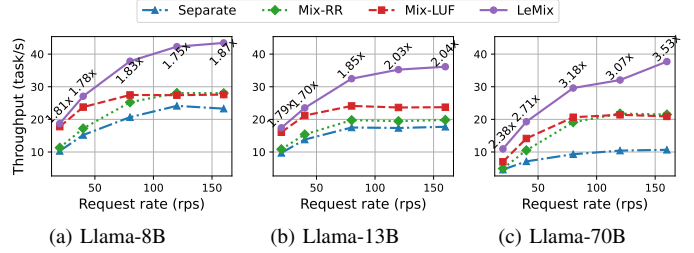


Fig. 11: Throughput (task/s) across various request rates.

- **MIX-LUF**: Lowest utilization first [50], serving as a strong baseline with more fine-grained execution awareness over RR, measures the GPU utilization and allocates tasks to nodes with the lowest average scores. MIX-LUF balances the active duration of all nodes over time, potentially preventing any single node from becoming a bottleneck.

### B. Results on Synthetic Workloads

We assess LEMIX and the baselines in three dimensions—*inference loss* of decoding human references to measure service quality under continuous retraining, *throughput* as a resource utilization metric when running mixed workloads, and *SLO attainment* to ensure prompt service responsiveness, under a spectrum of training rates for multiple models at different request rates on a four-node cluster.

**Improved serving quality under retraining.** Figure 10 shows Llama models’ average inference loss when running concurrent serving and training workloads. We observe a general decreasing loss under larger training rates, as the model are retrained on more samples. All mixed approaches achieve a lower loss compared to SEPARATE due to continuous updates from retraining (§III-A), with LEMIX consistently outperforming the others, reducing the average loss by up to  $0.61\times$  over SEPARATE. This superiority indicates that our idea of workload co-location and consideration of LC (§IV-C) in LEMIX benefits the training procedure and convergence. The discrepancy between SEPARATE and co-location methods gets larger as model sizes grow, due to prolonged inter-node weight synchronization latencies (§III-A).

**Throughput under varying traffic intensity.** Figure 11 shows Llama models’ throughput at various request rates when processing concurrent mixed workloads. We observe a notable enhance in resource efficiency for all methods at higher request rates, where LEMIX achieves the overall highest scores, improving throughput by up to  $3.53\times$  over SEPARATE. Particularly, MIX-LUF also excels under light

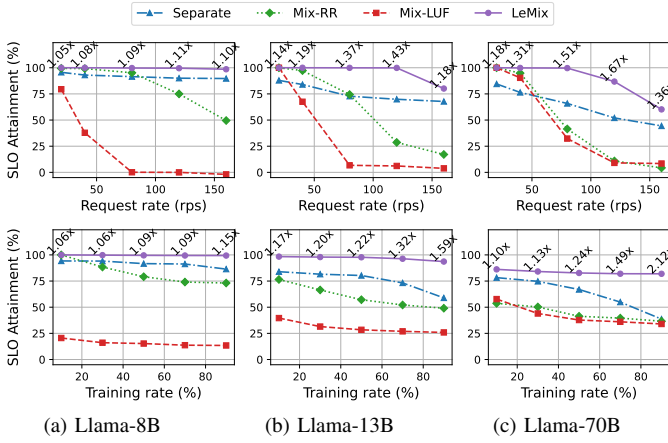


Fig. 12: SLO attainment under various request and training rates.

traffic conditions (e.g., less than 50 rps), which demonstrates the benefit of execution awareness in optimizing resource efficiency (§III-B), though such improvement over NAIVEMIX diminishes in rapid task arrival due to the time-intensive GPU utilization querying procedure (Table III) that significantly delays task execution. Moreover, the advantage of mixed methods over SEPARATE is pronounced for larger models at high request rates, as the execution delays caused by workload heterogeneity are amplified under these circumstances (§II).

**SLO attainment in varying conditions.** Figure 12 demonstrates a decreasing SLO attainment for Llama models as request rates (top row) and training rates (bottom row) increase. LEMIX consistently outperforms alternative methods, maintaining high SLO compliance across workload spectrum. This resilience stems from its dynamic latency-aware scheduling which reduces response times for inference tasks. In contrast, other mixed approaches suffer significant drop in SLO attainment, particularly at higher request rates, as co-locating workloads exacerbates contention for shared resources, delaying inference execution (§III-B). While SEPARATE achieves comparable performance to LEMIX under low workloads, its static property leads to declines in SLO compliance under higher training rates or request intensities. The performance gap widens with larger model sizes (e.g., Llama-70B), where LEMIX achieves up to 2.12 $\times$  better SLO attainment over SEPARATE at high training rates, indicating its scalability in managing heterogeneous workloads.

### C. Breakdown Analysis on Real Workloads

We constructed real workload traces from LMSYS platforms following a similar process in [29], where we treat each LLM as a client and sample requests from the trace and re-scale the real-time stamps to a time window. During this serving window, training samples from the datasets are mixed to form in total 1,000 samples with varying training rates. We evaluate node-level breakdown of *E2E latencies* and *response time* for LEMIX and the baselines.

**E2E latencies across nodes.** Figure 13 shows GPT models’ E2E latencies breakdown on each node when processing real workloads. We observe a clear increased latency when

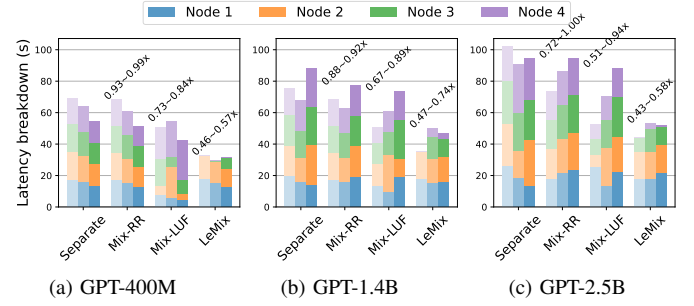


Fig. 13: Breakdown E2E latencies under training rates of 10% (light), 50% (medium), and 90% (dark color).

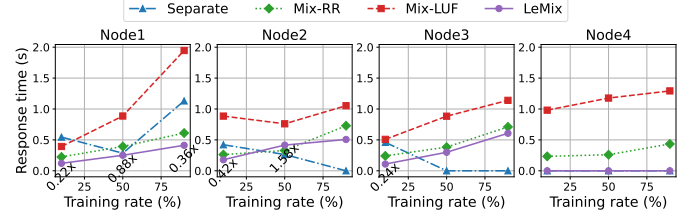


Fig. 14: Breakdown average response time on each node. Zero values mean no inference workloads are allocated on that node.

running larger models due to more computational demands. All mixed approaches require less time than SEPARATE to operate concurrent workloads, especially for larger models (e.g., GPT-2.5B) where workload heterogeneity amplifies the pipeline idleness of SEPARATE (§II). LEMIX achieves the lowest accumulative latencies, reducing the scores by up to 0.43 $\times$  over SEPARATE. One notable reason behind such gain is its ability to “dynamically” adjust resource allocation (§IV-C) based on real-time conditions. For examples, LEMIX allocates only 2 nodes when running two smaller models under lower training rates (e.g., 10%), effectively mitigating the sparsity issue in low workload demands.

**Response time across nodes.** Figure 14 details Llama-8B’s average response time (TTFT) on four nodes across various training rates. By default, Node 1 is dedicated to inference workloads in SEPARATE, where LEMIX achieves lower response times, reducing the average scores by up to 0.22 $\times$ . Such efficiency gain is more obvious under larger training rates where inference execution delays on Node 1 in SEPARATE are amplified due to overloaded requests. For the remaining three nodes, LEMIX still achieves the lowest response latencies under lower training rates (e.g., less than 50%), while SEPARATE excels under larger training rates since few or even no inference workloads are allocated to those nodes (e.g., Node 3). MIX-LUF exhibits significant response delays due to the latency of querying GPU utilization, indicating its limited practical applicability when SLO attainment is pursued.

### D. Impact of Workload Heterogeneity

Rapid task arrival combined with larger workload heterogeneity could result in substantial idleness (§II) and hampered training convergence (§IV-C) when operating synthetic workloads. To explore how LEMIX handles this property inherent

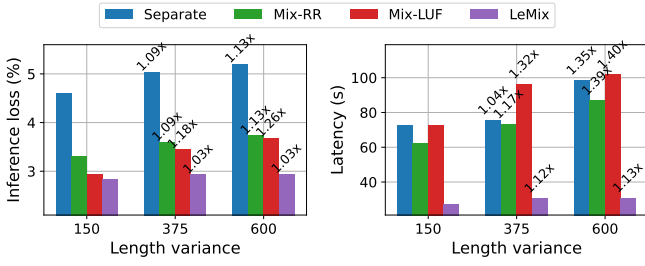


Fig. 15: Impact of length heterogeneity on *Left*: inference loss and *Right*: E2E latencies under heavy traffic (150 rps).

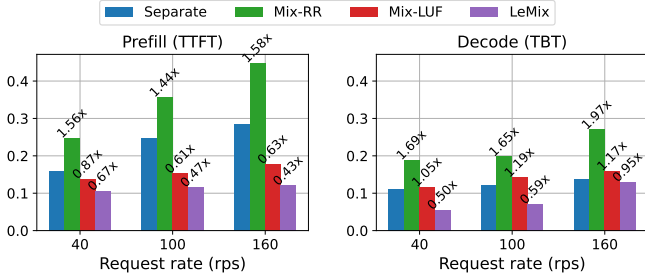


Fig. 16: *Left*: prefill and *Right*: decode latency of inference serving under various request rates for GPT-2.5B.

in real-world workloads, we simulate a range of length heterogeneities by sampling subsets from the two datasets. We run GPT-2.5B model on each subset under a request rate of 150 rps across various training rates. Figure 15 demonstrates a general increase in loss and E2E latency for LEMIX and the baselines as length heterogeneity grows. LEMIX is more robust against workload heterogeneity compared to the baseline methods: with up to  $1.03\times$  increase in inference loss and the maximum latency gain is  $1.13\times$ . This suggests that task-specific resource allocation can effectively mitigate the idleness incurred by co-execution interference and training inconsistency caused by workload heterogeneity.

#### E. Inference (Generation) Efficiency Study

To independently study inference latency under mixed training workloads, we run GPT-2.5B with a memory pool size of 1000 tokens allocated for KV cache [41] across various request rates with 50% training rate. Figure 16 highlights the performance variations across methods in both prefilling and decoding phases. LEMIX consistently achieves the lowest latency in both TTFT and TBT across all request rates, achieving up to  $0.43\times$  lower TTFT and  $0.50\times$  lower TBT compared to SEPARATE. Both MIX-LUF and NAIVEMIX incurs additional serving latency when co-locating serving and training workloads due to resource contention, and their TBT discrepancies are caused by the hybrid batches of both prefilling and decoding requests where node allocation (§IV-C) makes difference. MIX-LUF exhibits relatively better TTFT performance as the computation-intensive prefilling workloads are allocated to low-utilization nodes, but its TBT latency becomes a bottleneck due to frequent GPU utilization tracking during decoding. LEMIX dynamically allocates prefilling

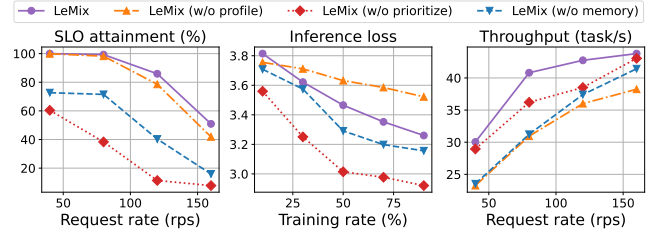


Fig. 17: Ablation analysis of LEMIX's components.

workloads across nodes (§IV-C) to prevent resource bottlenecks and cut TTFT latency, and leverages runtime scheduling (§IV-D) to fill idle GPU slots and use batching opportunities to minimize TBT during decoding. This adaptability ensures balanced resource utilization across computation- (prefill) and memory-bound (decode) phases, allowing LEMIX to excel in diverse conditions.

#### F. Understanding LEMIX's Improvements

We run Llama-70B on synthetic workloads across varying request and training rates to evaluate the contributions of individual components in LEMIX and their overheads.

**Robustness to offline priors.** LEMIX employs offline profiling (§IV-A) to improve the planning precision of execution latencies and memory demands, which enhances resource utilization. As shown in Figure 17, removing offline profiling (w/o profile) causes notable decrease in throughput, dropping by up to  $0.82\times$  compared to the full LEMIX design, particularly under high request rates when misjudgments tend to be accumulated. Inference loss also increases from 3.3 to 3.6 at 75% training rate due to potential update delays for inference tasks. Despite these setbacks, LEMIX (w/o profile) still outperforms baseline methods in higher throughput and SLO attainment due to fine-grained scheduling. This robustness to profiling accuracy highlights LEMIX's applicability even when offline resources are limited.

**Prioritization in responsiveness.** Queue-level task prioritization (§IV-C) in LEMIX is essential for meeting SLOs under high request rates. As shown in Figure 17, removing prioritization (w/o prioritize) causes SLO attainment to collapse drastically from 95% to below 30% at 100 rps and further plummeting to 0% at 150 rps. This is caused by the uncontrolled interference from training tasks which delay inference requests. LEMIX, in contrast, dynamically deprioritizes training tasks that risk SLO breaches, maintaining SLO attainment above 50% and improving throughput across the workload spectrum. Additionally, its slight drop in loss suggests the strength of dynamic scheduling where deprioritization sacrifices short-term accuracy improvements to ensure responsiveness.

**Memory awareness in efficiency.** Memory-aware scheduling (§IV-D) enables LEMIX to adaptively manage GPU resources and prevent memory overruns, ensuring system responsiveness. When memory awareness is disabled (w/o memory), SLO attainment degrades significantly, dropping from 95% to

	Separate	RR	LUF	LEMIX		
				EP	RA	MS
Latency (ms)	1.4e-2	1.5e-2	76	1.4e-1	1.4e-2	5.6e-2
Memory (MB)	1.6	1.8	727.5	9.6	1.9	1.8

TABLE III: Average time overhead (ms) and memory (MB) of schedulers. EP, RA, MS represents execution planning, resource allocation, and memory-aware scheduling.

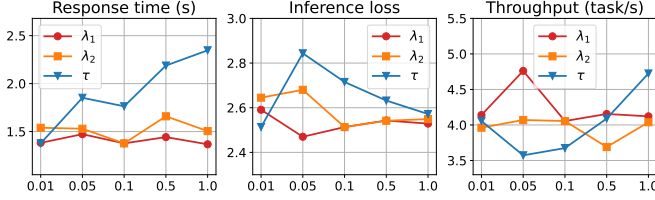


Fig. 18: Trade-offs in LEMIX's multi-objective allocation.

55% at 100 rps, as shown in Figure 17. Consequently, throughput drops from 8 to 6 at 80 rps due to memory-induced latency. By proactively offloading activations and enforcing memory thresholds, the full LEMIX ensures stable performance across diverse workloads while balancing resource demands.

**Overhead analysis.** Table III shows the average latency and memory usage under a request rate of 50 rps and training rate of 50%. LEMIX achieves its scheduling improvements with minimal computational cost. Specifically, execution planning incurs an average latency of 0.14 ms, slightly higher than simpler policies like RR, but still negligible compared to the model forward latency (Table II). Meanwhile, resource allocation and scheduling achieve latency comparable to RR, ensuring real-time responsiveness. Memory usage remains similarly efficient. While methods like LUF incur high overhead (727.5 MB) due to system-level GPU utilization tracking, LEMIX remains lightweight, consuming only 9.6 MB for its execution prediction and less than 4 MB for other modules. This efficient nature of LEMIX ensures scalability under heavy traffic conditions and supports real-time decision-making without introducing performance bottlenecks.

### G. Parameter Study

Figure 18 illustrates the trade-offs between response time, serving quality (inference loss), and throughput under varying priority weights ( $\lambda_1$ ,  $\lambda_2$ ) and idleness tolerance threshold ( $\tau$ ) in LEMIX's resource allocation. Increasing  $\lambda_1$  (response time weight) reduces latency by prioritizing faster execution but limits resource utilization, while higher  $\lambda_2$  (length consistency weight) improves serving quality by reducing workload heterogeneity at the cost of slight delays. Meanwhile, larger  $\tau$  allows better idle-period utilization and higher throughput by consolidating workloads to fewer nodes, but risks prolonged response times as tasks wait for resources. Overall, LEMIX achieves a robust balance with “sweet spots” of  $\lambda_1$ ,  $\lambda_2$ , and  $\tau$ : it maintains low response times (e.g., 150 ms), high throughput (e.g., 4.5 task/s), and stable inference quality (e.g., 2.5), showcasing its adaptability to dynamic real-time conditions.

## VII. RELATED WORK

**Distributed training.** Distributed training of large models has been extensively explored to address the computational demands of increasing complexity. Techniques such as data parallelism [51–53] where the data is split across multiple processors, model parallelism [20] where the model is horizontally sharded into multiple computational units, and pipeline parallelism [21, 25, 54, 55] which divides each input mini-batch into small micro-batches to further reduce idleness, are well-established. While these approaches optimize utilization, they leave inter-pipeline idle periods unaddressed.

**Inference serving.** LLM serving systems have evolved to tackle the dynamic requirements of LLM workloads. General-purpose systems [56–60] are widely used for production environments, while LLM-optimized systems [14, 61, 62] have emerged to handle KV cache management and chunked prefill processing. Techniques like Orca [17] and FastServe [63] introduce continuous batching and preemptive scheduling [12], addressing delays caused by long jobs, but often exacerbate interference when workloads are co-located. Furthermore, disaggregation-based approaches [13, 64, 65] reduce contention by isolating specific workload stages. Unlike these methods, LEMIX focuses on node allocation, idleness utilization, and retraining alignment, demonstrating compatibility with autoregressive generation.

**Data drift and continual learning.** Adapting to data drift [66, 67] has been widely studied in continuous learning scenarios, where models evolve with new incoming data. Traditional methods include transfer learning [4, 32, 68] and catastrophic forgetting mitigation [69–71], while edge deployment systems [72–74] demonstrate scheduling techniques for model retraining. Inference serving for LLMs also faces challenges similar to data drift, as models require frequent alignment to updated user interactions and factual knowledge. LEMIX builds upon continuous learning principles by co-locating training and inference workloads, enabling real-time adaptation with reduced inter-node synchronization delays, which is critical for emerging “learning while serving” paradigms.

## VIII. CONCLUSION

In this work, we introduced LEMIX, a framework that schedules concurrent LLM training and inference workloads in distributed systems. The key innovation is exploring optimizations when co-locating both computational workloads under dynamic traffic and execution heterogeneity, and integrating these insights to optimize resource utilization while attaining SLOs. By real-time quantifying task-specific contributions to idle periods, accuracy, and response time, LEMIX achieves up to  $3.53\times$  higher throughput,  $0.61\times$  lower loss, and  $2.12\times$  higher SLO attainment over traditional SEPARATE setups.

## ACKNOWLEDGMENT

This research was supported by the National Science Foundation under NSF CNS 2300525, CNS 2343653, CNS 2312397.



## REFERENCES

- [1] J. Wei, X. Wang, D. Schuurmans, M. Bosma, F. Xia, E. Chi, Q. V. Le, D. Zhou *et al.*, “Chain-of-thought prompting elicits reasoning in large language models,” *Advances in neural information processing systems*, vol. 35, pp. 24 824–24 837, 2022.
- [2] S. Yao, D. Yu, J. Zhao, I. Shafran, T. Griffiths, Y. Cao, and K. Narasimhan, “Tree of thoughts: Deliberate problem solving with mt-bench and chatbot arena,” *Advances in Neural Information Processing Systems*, vol. 36, 2024.
- [3] L. Zheng, W.-L. Chiang, Y. Sheng, S. Zhuang, Z. Wu, Y. Zhuang, Z. Lin, Z. Li, D. Li, E. Xing *et al.*, “Judging llm-as-a-judge with mt-bench and chatbot arena,” *Advances in Neural Information Processing Systems*, vol. 36, 2024.
- [4] Y. Sun, X. Wang, Z. Liu, J. Miller, A. Efros, and M. Hardt, “Test-time training with self-supervision for generalization under distribution shifts,” in *International conference on machine learning*. PMLR, 2020, pp. 9229–9248.
- [5] E. Akyürek, M. Damani, L. Qiu, H. Guo, Y. Kim, and J. Andreas, “The surprising effectiveness of test-time training for abstract reasoning,” *arXiv preprint arXiv:2411.07279*, 2024.
- [6] Langton, “Machine learning model training over time,” May 2018. [Online]. Available: <https://www.langton.cloud/machine-learning-model-training-over-time/>
- [7] S. Choi, S. Lee, Y. Kim, J. Park, Y. Kwon, and J. Huh, “Multi-model machine learning inference serving with gpu spatial partitioning,” *arXiv preprint arXiv:2109.01611*, 2021.
- [8] A. Vilcek, “Optimized training and inference of hugging face models on azure,” September 2022. [Online]. Available: <https://techcommunity.microsoft.com/t5/microsoft-developer-community/optimized-training-and-inference-of-hugging-face-models-on-azure/ba-p/3631401>
- [9] Amazon Web Services, Inc., “Train a model with amazon sagemaker,” <https://docs.aws.amazon.com/sagemaker/latest/dg/how-it-works-training.html>, Amazon Web Services, Inc., 2024, accessed: 2024-05-12.
- [10] S. Choi, S. Lee, Y. Kim, J. Park, Y. Kwon, and J. Huh, “Serving heterogeneous machine learning models on Multi-GPU servers with Spatio-Temporal sharing,” in *2022 USENIX Annual Technical Conference (USENIX ATC 22)*. Carlsbad, CA: USENIX Association, Jul. 2022, pp. 199–216.
- [11] W. Kwon, Z. Li, S. Zhuang, Y. Sheng, L. Zheng, C. H. Yu, J. Gonzalez, H. Zhang, and I. Stoica, “Efficient memory management for large language model serving with pagedattention,” in *Proceedings of the 29th Symposium on Operating Systems Principles*, 2023, pp. 611–626.
- [12] B. Sun, Z. Huang, H. Zhao, W. Xiao, X. Zhang, Y. Li, and W. Lin, “Llumnix: Dynamic scheduling for large language model serving,” in *18th USENIX Symposium on Operating Systems Design and Implementation (OSDI 24)*, 2024.
- [13] Y. Zhong, S. Liu, J. Chen, J. Hu, Y. Zhu, X. Liu, X. Jin, and H. Zhang, “[DistServe]: Disaggregating prefill and decoding for goodput-optimized large language model serving,” in *18th USENIX Symposium on Operating Systems Design and Implementation (OSDI 24)*, 2024, pp. 193–210.
- [14] A. Agrawal, N. Kedia, A. Panwar, J. Mohan, N. Kwatra, B. Gulavani, A. Tumanov, and R. Ramjee, “Taming {Throughput-Latency} tradeoff in {LLM} inference with {Sarathi-Serve},” in *18th USENIX Symposium on Operating Systems Design and Implementation (OSDI 24)*, 2024, pp. 117–134.
- [15] B. Wu, R. Zhu, Z. Zhang, P. Sun, X. Liu, and X. Jin, “[dLoRA]: Dynamically orchestrating requests and adapters for {LoRA}{LLM} serving,” in *18th USENIX Symposium on Operating Systems Design and Implementation (OSDI 24)*, 2024, pp. 911–927.
- [16] Y. Fu, L. Xue, Y. Huang, A.-O. Brabete, D. Ustiugov, Y. Patel, and L. Mai, “[ServerlessLLM]: {Low-Latency} serverless inference for large language models,” in *18th USENIX Symposium on Operating Systems Design and Implementation (OSDI 24)*, 2024, pp. 135–153.
- [17] G.-I. Yu, J. S. Jeong, G.-W. Kim, S. Kim, and B.-G. Chun, “Orca: A distributed serving system for Transformer-Based generative models,” in *16th USENIX Symposium on Operating Systems Design and Implementation (OSDI 22)*. Carlsbad, CA: USENIX Association, Jul. 2022, pp. 521–538.
- [18] A. L. Gaunt, M. A. Johnson, M. Riechert, D. Tarlow, R. Tomioka, D. Vytiniotis, and S. Webster, “Ampnet: Asynchronous model-parallel training for dynamic neural networks,” *arXiv preprint arXiv:1705.09786*, 2017.
- [19] D. Narayanan, A. Harlap, A. Phanishayee, V. Seshadri, N. R. Devanur, G. R. Ganger, P. B. Gibbons, and M. Zaharia, “Pipedream: generalized pipeline parallelism for dnn training,” in *Proceedings of the 27th ACM symposium on operating systems principles*, 2019, pp. 1–15.
- [20] M. Shoenybi, M. Patwary, R. Puri, P. LeGresley, J. Casper, and B. Catanzaro, “Megatron-lm: Training multi-billion parameter language models using model parallelism,” *arXiv preprint arXiv:1909.08053*, 2019.
- [21] S. Athlur, N. Saran, M. Sivathanu, R. Ramjee, and N. Kwatra, “Varuna: scalable, low-cost training of massive deep learning models,” in *Proceedings of the Seventeenth European Conference on Computer Systems*, 2022, pp. 472–487.
- [22] S. Choi, I. Koo, J. Ahn, M. Jeon, and Y. Kwon, “[EnvPipe]: Performance-preserving {DNN} training framework for saving energy,” in *2023 USENIX Annual Technical Conference (USENIX ATC 23)*, 2023, pp. 851–864.
- [23] Z. Li, L. Zheng, Y. Zhong, V. Liu, Y. Sheng, X. Jin, Y. Huang, Z. Chen, H. Zhang, J. E. Gonzalez *et al.*, “[AlpaServe]: Statistical multiplexing with model parallelism for deep learning serving,” in *17th USENIX Symposium on Operating Systems Design and Implementation (OSDI 23)*, 2023, pp. 663–679.
- [24] Z. Lai, S. Li, X. Tang, K. Ge, W. Liu, Y. Duan, L. Qiao, and D. Li, “Merak: An efficient distributed dnn training framework with automated 3d parallelism for giant foundation models,” *IEEE Transactions on Parallel and Distributed Systems*, vol. 34, no. 5, pp. 1466–1478, 2023.
- [25] Y. Huang, Y. Cheng, A. Bapna, O. Firat, D. Chen, M. Chen, H. Lee, J. Ngiam, Q. V. Le, Y. Wu *et al.*, “Gpipe: Efficient training of giant neural networks using pipeline parallelism,” *Advances in neural information processing systems*, vol. 32, 2019.
- [26] H. Touvron, L. Martin, K. Stone, P. Albert, A. Almahairi, Y. Babaei, N. Bashlykov, S. Batra, P. Bhargava, S. Bhosale *et al.*, “Llama 2: Open foundation and fine-tuned chat models,” *arXiv preprint arXiv:2307.09288*, 2023.
- [27] L. Zheng, W.-L. Chiang, Y. Sheng, T. Li, S. Zhuang, Z. Wu, Y. Zhuang, Z. Li, Z. Lin, E. Xing *et al.*, “Lmsys-chat-1m: A large-scale real-world llm conversation dataset,” in *The Twelfth International Conference on Learning Representations*, 2023.
- [28] L. Zheng, W.-L. Chiang, Y. Sheng, S. Zhuang, Z. Wu, Y. Zhuang, Z. Lin, Z. Li, D. Li, E. Xing *et al.*, “Judging llm-as-a-judge with mt-bench and chatbot arena,” *Advances in Neural Information Processing Systems*, vol. 36, pp. 46 595–46 623, 2023.
- [29] Y. Sheng, S. Cao, D. Li, B. Zhu, Z. Li, D. Zhuo, J. E. Gonzalez, and I. Stoica, “Fairness in serving large language models,” in *18th USENIX Symposium on Operating Systems Design and Implementation (OSDI 24)*, 2024, pp. 965–988.
- [30] Y. Shen, J. Shao, X. Zhang, Z. Lin, H. Pan, D. Li, J. Zhang, and K. B. Letaief, “Large language models empowered autonomous edge ai for connected intelligence,” *IEEE Communications Magazine*, 2024.
- [31] P. F. Christiano, J. Leike, T. Brown, M. Martic, S. Legg, and D. Amodei, “Deep reinforcement learning from human preferences,” *Advances in neural information processing systems*, vol. 30, 2017.
- [32] Y. Li, J. Nham, G. Jawahar, L. Shu, D. Uthus, Y.-H. Sung, C. Yang, I. Rolnick, Y. Qiao, and C. Liu, “Dr genre: Reinforcement learning from decoupled llm feedback for generic text rewriting,” *arXiv preprint arXiv:2503.06781*, 2025.
- [33] J. Dai, X. Pan, R. Sun, J. Ji, X. Xu, M. Liu, Y. Wang, and Y. Yang, “Safe rlhf: Safe reinforcement learning from human feedback,” in *The Twelfth International Conference on Learning Representations*, 2023.
- [34] Y. Fu, Y. Li, W. Xiao, C. Liu, and Y. Dong, “Safety alignment in nlp tasks: Weakly aligned summarization as an in-context attack,” in *Proceedings of the 62nd Annual Meeting of the Association for Computational Linguistics (Volume 1: Long Papers)*, 2024, pp. 8483–8502.
- [35] Z. Jia, M. Zaharia, and A. Aiken, “Beyond data and model parallelism for deep neural networks,” *Proceedings of Machine Learning and Systems*, vol. 1, pp. 1–13, 2019.
- [36] GPT AI Team, “How many servers are needed to run chatgpt?” Aug. 2024, accessed: 2024-12-05. [Online]. Available: <https://gptai.tn/how-many-servers-to-run-chatgpt/>
- [37] Y. Bai, A. Jones, K. Ndousse, A. Askell, A. Chen, N. DasSarma, D. Drain, S. Fort, D. Ganguli, T. Henighan *et al.*, “Training a helpful and harmless assistant with reinforcement learning from human feedback,” *arXiv preprint arXiv:2204.05862*, 2022.

- [38] K. Ethayarajh, Y. Choi, and S. Swayamdipta, "Understanding dataset difficulty with  $\mathcal{V}$ -usable information," in *Proceedings of the 39th International Conference on Machine Learning*, ser. Proceedings of Machine Learning Research, vol. 162. PMLR, 17–23 Jul 2022, pp. 5988–6008.
- [39] A. Vaswani, N. Shazeer, N. Parmar, J. Uszkoreit, L. Jones, A. N. Gomez, Ł. Kaiser, and I. Polosukhin, "Attention is all you need," *Advances in neural information processing systems*, vol. 30, 2017.
- [40] B. Wu, Z. Zhang, Z. Bai, X. Liu, and X. Jin, "Transparent {GPU} sharing in container clouds for deep learning workloads," in *20th USENIX Symposium on Networked Systems Design and Implementation (NSDI 23)*, 2023, pp. 69–85.
- [41] R. Pope, S. Douglas, A. Chowdhery, J. Devlin, J. Bradbury, J. Heek, K. Xiao, S. Agrawal, and J. Dean, "Efficiently scaling transformer inference," *Proceedings of Machine Learning and Systems*, vol. 5, pp. 606–624, 2023.
- [42] B. Reagen, Y. S. Shao, S. L. Xi, G.-Y. Wei, and D. Brooks, "Methods and infrastructure in the era of accelerator-centric architectures," in *2017 IEEE 60th International Midwest Symposium on Circuits and Systems (MWSCAS)*. IEEE, 2017, pp. 902–905.
- [43] Y. Li, Z. Li, W. Yang, and C. Liu, "Rt-lm: Uncertainty-aware resource management for real-time inference of language models," in *2023 IEEE Real-Time Systems Symposium (RTSS)*. IEEE, 2023, pp. 158–171.
- [44] Z. Li, J. Zhang, Y. Li, Y. Zhu, and C. Liu, "Mixtraining: A better trade-off between compute and performance," *arXiv preprint arXiv:2502.19513*, 2025.
- [45] L. Zheng, L. Yin, Z. Xie, C. L. Sun, J. Huang, C. H. Yu, S. Cao, C. Kozyrakis, I. Stoica, J. E. Gonzalez *et al.*, "Sglang: Efficient execution of structured language model programs," *Advances in neural information processing systems*, vol. 37, pp. 62 557–62 583, 2024.
- [46] A. Eisenman, K. K. Matam, S. Ingram, D. Mudigere, R. Krishnamoorthi, K. Nair, M. Smelyanskiy, and M. Annavaram, "{Check-N-Run}: A checkpointing system for training deep learning recommendation models," in *19th USENIX Symposium on Networked Systems Design and Implementation (NSDI 22)*, 2022, pp. 929–943.
- [47] R. Y. Aminabadi, S. Rajbhandari, A. A. Awan, C. Li, D. Li, E. Zheng, O. Ruwase, S. Smith, M. Zhang, J. Rasley *et al.*, "DeepSpeed-Inference: enabling efficient inference of transformer models at unprecedented scale," in *SC22: International Conference for High Performance Computing, Networking, Storage and Analysis*. IEEE, 2022, pp. 1–15.
- [48] T. Dao, D. Fu, S. Ermon, A. Rudra, and C. Ré, "Flashattention: Fast and memory-efficient exact attention with io-awareness," *Advances in neural information processing systems*, vol. 35, pp. 16 344–16 359, 2022.
- [49] Y. Zhang, S. Sun, M. Galley, Y.-C. Chen, C. Brockett, X. Gao, J. Gao, J. Liu, and W. B. Dolan, "Dialogpt: Large-scale generative pre-training for conversational response generation," in *Proceedings of the 58th Annual Meeting of the Association for Computational Linguistics: System Demonstrations*, 2020, pp. 270–278.
- [50] S. Feizabadi, W. Beebe Jr, B. Ravindran, P. Li, and M. Rinard, "Utility accrual scheduling with real-time java," in *OTM Confederated International Conferences "On the Move to Meaningful Internet Systems"*. Springer, 2003, pp. 550–563.
- [51] A. Sergeev and M. Del Balso, "Horovod: fast and easy distributed deep learning in tensorflow," *arXiv preprint arXiv:1802.05799*, 2018.
- [52] Y. Jiang, Y. Zhu, C. Lan, B. Yi, Y. Cui, and C. Guo, "A unified architecture for accelerating distributed {DNN} training in heterogeneous {GPU/CPU} clusters," in *14th USENIX Symposium on Operating Systems Design and Implementation (OSDI 20)*, 2020, pp. 463–479.
- [53] J. Dean, G. Corrado, R. Monga, K. Chen, M. Devin, M. Mao, M. Ranzato, A. Senior, P. Tucker, K. Yang *et al.*, "Large scale distributed deep networks," *Advances in neural information processing systems*, vol. 25, 2012.
- [54] S. Li and T. Hoefler, "Chimera: efficiently training large-scale neural networks with bidirectional pipelines," in *Proceedings of the International Conference for High Performance Computing, Networking, Storage and Analysis*, 2021, pp. 1–14.
- [55] K. Osawa, S. Li, and T. Hoefler, "Pipefisher: Efficient training of large language models using pipelining and fisher information matrices," *Proceedings of Machine Learning and Systems*, vol. 5, 2023.
- [56] L. Ning, H. Shojanazeri, K. Wen, and the PyTorch Foundation, "Torchserve: Serve, optimize and scale pytorch models in production," PyTorch Foundation, 2023, <https://pytorch.org/serve/>.
- [57] NVIDIA Corporation, "Triton inference server: An optimized cloud and edge inferencing solution," 2019, <https://developer.nvidia.com/nvidia-triton-inference-server>.
- [58] Y. Li, Z. Li, Y. Gao, and C. Liu, "White-box multi-objective adversarial attack on dialogue generation," in *Proceedings of the 61st Annual Meeting of the Association for Computational Linguistics (Volume 1: Long Papers)*, 2023, pp. 1778–1792.
- [59] S. Chen, S. Wei, C. Liu, and W. Yang, "DyCl: Dynamic neural network compilation via program rewriting and graph optimization," in *Proceedings of the 32nd ACM SIGSOFT International Symposium on Software Testing and Analysis*, 2023, pp. 614–626.
- [60] S. Chen, H. Khanpour, C. Liu, and W. Yang, "Learning to reverse dnns from ai programs automatically," *arXiv preprint arXiv:2205.10364*, 2022.
- [61] D. Narayanan, M. Shoenybi, J. Casper, P. LeGresley, M. Patwary, V. Korthikanti, D. Vainbrand, P. Kashinkunti, J. Bernauer, B. Catanzaro *et al.*, "Efficient large-scale language model training on gpu clusters using megatron-lm," in *Proceedings of the International Conference for High Performance Computing, Networking, Storage and Analysis*, 2021, pp. 1–15.
- [62] X. Li, Y. Ma, Y. Huang, X. Wang, Y. Lin, and C. Zhang, "Integrated optimization of large language models: Synergizing data utilization and compression techniques," 2024.
- [63] B. Wu, Y. Zhong, Z. Zhang, S. Liu, F. Liu, Y. Sun, G. Huang, X. Liu, and X. Jin, "Fast distributed inference serving for large language models," *arXiv preprint arXiv:2305.05920*, 2023.
- [64] P. Patel, E. Choukse, C. Zhang, A. Shah, Í. Goiri, S. Maleki, and R. Bianchini, "Splitwise: Efficient generative llm inference using phase splitting," in *2024 ACM/IEEE 51st Annual International Symposium on Computer Architecture (ISCA)*. IEEE, 2024, pp. 118–132.
- [65] F. Strati, S. McAllister, A. Phanishayee, J. Tarnawski, and A. Klimovic, "Dějävü: KV-cache streaming for fast, fault-tolerant generative LLM serving," in *Proceedings of the 41st International Conference on Machine Learning*, ser. Proceedings of Machine Learning Research, R. Salakhutdinov, Z. Kolter, K. Heller, A. Weller, N. Oliver, J. Scarlett, and F. Berkenkamp, Eds., vol. 235. PMLR, 21–27 Jul 2024, pp. 46 745–46 771.
- [66] Y. Li, S. Chen, and W. Yang, "Estimating predictive uncertainty under program data distribution shift," *arXiv preprint arXiv:2107.10989*, 2021.
- [67] Y. Li, S. Chen, Y. Guo, W. Yang, Y. Dong, and C. Liu, "Uncertainty awareness of large language models under code distribution shifts: A benchmark study," *arXiv preprint arXiv:2402.05939*, 2024.
- [68] G. Hinton, O. Vinyals, and J. Dean, "Distilling the knowledge in a neural network," in *NeurIPS Deep Learning and Representation Learning Workshop*, 2015.
- [69] I. J. Goodfellow, M. Mirza, D. Xiao, A. Courville, and Y. Bengio, "An empirical investigation of catastrophic forgetting in gradient-based neural networks," *arXiv preprint arXiv:1312.6211*, 2013.
- [70] Y. Li, X. Yu, Y. Liu, H. Chen, and C. Liu, "Uncertainty-aware bootstrap learning for joint extraction on distantly-supervised data," in *Proceedings of the 61st Annual Meeting of the Association for Computational Linguistics (Volume 2: Short Papers)*, 2023, pp. 1349–1358.
- [71] Y. Li, X. Yu, Y. Guo, Y. Liu, H. Chen, and C. Liu, "Distantly-supervised joint extraction with noise-robust learning," in *Findings of the Association for Computational Linguistics ACL 2024*, 2024, pp. 10 202–10 217.
- [72] R. Bhardwaj, Z. Xia, G. Ananthanarayanan, J. Jiang, Y. Shu, N. Karianakis, K. Hsieh, P. Bahl, and I. Stoica, "Ekya: Continuous learning of video analytics models on edge compute servers," in *19th USENIX Symposium on Networked Systems Design and Implementation (NSDI 22)*, 2022, pp. 119–135.
- [73] S. S. Shubha and H. Shen, "Adainf: Data drift adaptive scheduling for accurate and slo-guaranteed multiple-model inference serving at edge servers," in *Proceedings of the ACM SIGCOMM 2023 Conference*, 2023, pp. 473–485.
- [74] J. Li, H. Xu, Y. Zhu, Z. Liu, C. Guo, and C. Wang, "Lyra: Elastic scheduling for deep learning clusters," in *Proceedings of the Eighteenth European Conference on Computer Systems*, 2023, pp. 835–850.